frontiers | Frontiers in Materials

ORIGINAL RESEARCH
published: 26 April 2022
doi: 10.3389/fmats.2022.896953

Multi-Tube Helmholtz Resonator Based Triboelectric Nanogenerator for Broadband Acoustic Energy Harvesting

*Qiqi Zhang, Ziyue Xi, Yawei Wang, Ling Liu, Hongyong Yu, Hao Wang and Minyi Xu**

Dalian Key Lab of Marine Micro/Nano Energy and Self-powered Systems, Marine Engineering College, Dalian Maritime University, Dalian, China

Acoustic energy, especially broadband low-frequency sound energy is part of the environmental mechanical energy acquisition cannot be ignored. Herein, a multi-tube parallel Helmholtz resonator-based triboelectric nanogenerator (MH-TENG) is investigated to reap sound energy in low-frequency noise environments. The designed MH-TENG consists of a modified Helmholtz resonator and a thin-film TENG transducer. The core materials of the TENG transducer are aluminum, FEP film, and carbon. To further clarify the influence of the modified Helmholtz resonator on the conversion performance of MH-TENG, the acoustic characteristics of the improved resonators are systematically studied. A series of experiments show that the multi-tube parallel Helmholtz resonator structure has a better sound wave collection effect. Meanwhile, the flexible film TENG can reduce the optimal output frequency of the device. The power generation performance and the bandwidth of the MH-TENG are significantly improved by adopting a multi-tube Helmholtz resonator. Within the frequency bandwidth range of 230 Hz, MH-TENG can effectively improve the efficiency of acoustic energy harvesting. 110 LEDs and an electronic thermometer can be powered by the sound-driven MH-TENG. In addition, the MH-TENG has a good capacitor charging performance, which is conducive to its application in ambient sound energy harvesting.

Keywords: acoustic energy harvesting, Helmholtz resonator, triboelectric nanogenerator, broadband, fluorinated ethylene propylene

OPEN ACCESS

Edited by:
Jiajia Shao,
Beijing Institute of Nanoenergy and Nanosystems CAS

Reviewed by:
Xiaoyi Li,
Ocean University of China, China
Haiyang Zou,
Georgia Institute of Technology, United States

****Correspondence:***
Minyi Xu
xuminyi@dlmu.edu.cn

Specialty section:
This article was submitted to Energy Materials, a section of the journal Frontiers in Materials

Received: *15 March 2022*
Accepted: *31 March 2022*
Published: *26 April 2022*

Citation:
Zhang Q, Xi Z, Wang Y, Liu L, Yu H, Wang H and Xu M (2022) Multi-Tube Helmholtz Resonator Based Triboelectric Nanogenerator for Broadband Acoustic Energy Harvesting. Front. Mater. 9:896953. doi: 10.3389/fmats.2022.896953

INTRODUCTION

Recently, the progress of electronic devices puts forward new requirements for energy supply, which are environmentally friendly, distributed, and low power consumption (Zhu et al., 2019). Therefore, collecting mechanical energy from surroundings comes to be a new way of small-scale energy supply (Luo and Wang, 2020; Song et al., 2021). As an extensively distributed vibration energy in the environment, the acoustic wave has recently attracted a lot of attention. Sound energy is widely generated around manufacturing industries and operating vehicles (Ali, 2011; Huabing et al., 2018), such as power plants, aluminum factories, diesel engines, and marine engine rooms. The sound pressure level (SPL) of these noisy environments even exceeds 115 dB, which is very conducive to gathering sound energy (JunHong and Bing, 2005).

In the actual environment, acoustic energy is mainly concentrated in the low-frequency range (Yuan et al., 2020). Low-frequency sound waves energy can be converted into electrical energy through appropriate energy conversion technology. At present, due to various energy conversion mechanisms, acoustic energy harvesting devices are mainly divided into electromagnetic generators (EMG) (Khan and Izhar, 2016; Izhar and Khan, 2018), piezoelectric generators (PEG) (Noh, 2018; Yuan et al., 2018; Iftikhar et al., 2019; Ji et al., 2020), and triboelectric nanogenerators (TENG) (Kim et al., 2015; Liu et al., 2016; Qiu et al., 2020; Wang et al., 2021). Compared with other generators, the TENG, based on thin-film vibration, has great acoustic impedance matching characteristics to achieve efficient energy harvesting (Cui et al., 2015; Yuan M. et al., 2021). The standardization of TENG also laid a good theoretical foundation for its application (Li et al., 2018). What's more, there is a wider range of materials available for TENG (Wang et al., 2015; Zou et al., 2020), which makes TENG more convenient to manufacture, lower cost, and broader in the application.

In recent years, several studies have confirmed the effectiveness and application potential of TENG in acoustic energy harvesting. Yang et al. developed the original sound-driven triboelectric nanogenerator based on organic film and a Helmholtz resonator (Yang et al., 2014). Although the sound wave is incident from the resonator backplate rather than the neck, and the resonator is underutilized, this proposed device inspired the successors to use TENG to gather sound energy. Afterward, Zhao et al. designed a modified sound-driven TENG based on a dual tubes parallel Helmholtz resonator to improve electrical output performance and accessible frequency bandwidth, while the SPL of the incident sound wave is measured at the resonator backplate rather than the neck tube (Zhao et al., 2019). Yuan et al. studied a conical cavity resonator TENG to enhance the performance of acoustic energy harvesting (Yuan H. et al., 2021). Results show that the generation performance can be improved by adjusting the shape and size of the cavity. These sound energy collection devices rely on typical Helmholtz resonators and their improved structures, which can enhance the excitation of sound waves. However, the typical Helmholtz resonator only amplifies the acoustic pressure in a narrow frequency range, which is not conducive to collecting acoustic energy in the environment. Therefore, it is significant to develop a new type of sound-driven TENG with a broadband sound pressure amplification device.

Herein, we propose a multi-tube parallel Helmholtz resonator TENG (MH-TENG), in which a four-tube Helmholtz resonator and a thin-film TENG act as a sound pressure amplifier and an energy transducer, respectively. Fluorinated ethylene propylene (FEP) and aluminum are the friction materials of the TENG transducer, while conductive ink (carbon) and aluminum are used as electrodes. Driven by the sound pressure difference inbetween the cavity, the FEP film alternately contacts and separates from aluminum, and then alternating current is generated. The acoustic characteristics of the multi-tube Helmholtz resonator are systematically investigated. Furthermore, the electricity generation performances of the MH-TENG are also experimentally studied. Results confirm that the electricity generation performances and accessible bandwidth of the MH-TENG are significantly improved. Compared with Helmholtz resonator TENGs of a single tube and dual-tube, the working frequency bandwidth of MH-TENG has been widened by 130 and 77%, respectively. What's more, the MH-TENG has a good capacitor charging performance, which can supply power for a small electronic thermometer in noisy environments.

RESULTS AND DISCUSSION

Component Design and Working Principle of Multi-Tube Parallel Helmholtz Resonator-Based Triboelectric Nanogenerator

The designed MH-TENG is composed of an improved multi-tube Helmholtz resonator and an energy transducer based on thin-film TENG. **Figure 1A** displays the component design diagram of the MH-TENG. The thin-film TENG is embedded on the backplate of the resonator. The improved Helmholtz resonator is made by a 3D printer with the material of degradable polylactic acid (PLA). The cavity size of the Helmholtz resonator is 72 * 72 * 40 mm, the radius of the neck tube is 5 mm, and the length is 30 mm. **Figure 1B** shows the component details and material selection of the TENG transducer device. The bottom of the device adopts a perforated square plate, which is printed by PLA material. The 50 μm thick perforated aluminum film is pasted on the PLA plate. The middle part is an acrylic gasket, which ensures the effective contact-separation space of the upper and lower friction layer materials. The upper part is a 30 μm thick FEP film with conductive ink printed on the back.

In general, the sound wave propagates through the acoustic holes of the PLA-Al plate and excites the PEP film to vibrate. The acoustic holes with 2 mm aperture are located at the edge of the plate, and those with 1 mm aperture are distributed inside the plate. Due to the film tension and gasket gap, the FEP film at the edge of the plate does not contact the aluminum film, so the larger acoustic holes are used to connect the air. While the size of the acoustic hole in the middle area is small, which is conducive to balancing the contact area and airflow. Relevant studies show that a smaller acoustic hole size will increase acoustic viscosity loss and thermoacoustic loss (Dukhin and Goetz, 2009). Specifically, the thickness of the acoustic viscous boundary layer of 100 Hz sound waves in air is 0.22 mm. And this thickness will increase to 0.5 mm as the acoustic frequency decreases to 20 Hz. Consequently, it is necessary to set an appropriate acoustic hole size.

In the light of the triboelectric series (Zou et al., 2019), aluminum is a kind of good positive triboelectric material, which is used as both a friction layer and an electrode in this work. FEP is a good negative triboelectric material with a powerful ability to capture electrons from other materials. Therefore, FEP film is used as another friction layer. To maintain the great flexibility of FEP film, conductive ink,

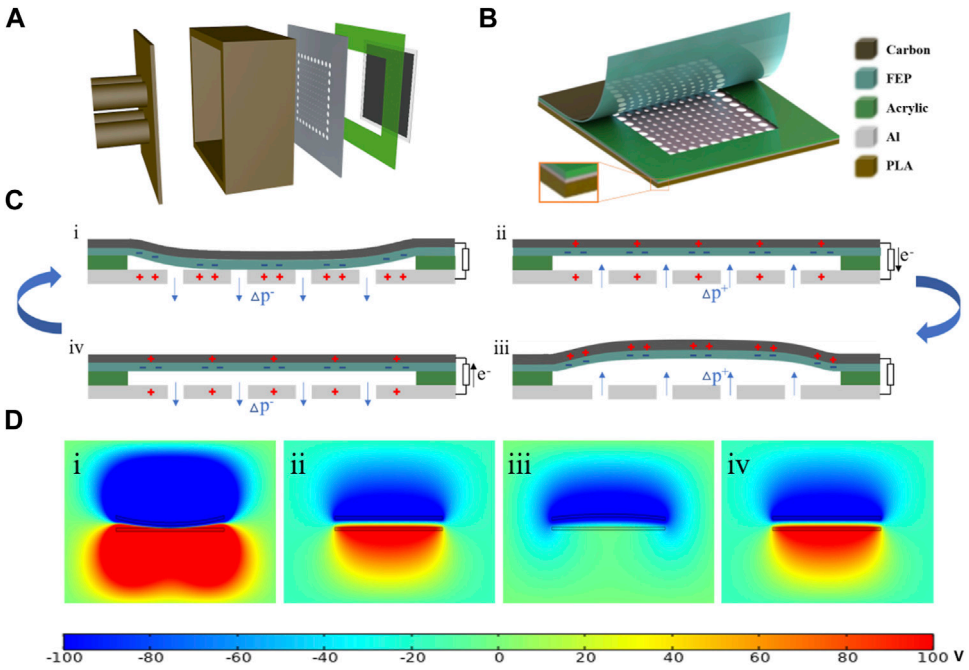

FIGURE 1 | (A) Component design of the MH-TENG **(B)** Component details diagram and material selection of TENG transducer device **(C)** Working principle diagram of the TENG transducer in one working cycle **(D)** Potential simulations of two friction interfaces of a TENG transducer by COMSOL.

which main conductive component is carbon, as another electrode is prepared on the back of FEP film by the screen-printing process. Furthermore, the microstructure of the friction material interface can effectively enlarge the friction contact area and contact stress of friction material, which is conducive to generating more charges (Zou et al., 2021). In short, that is an effective way to enhance TENG output, referring to the following equation:

$$V_{oc} = \frac{\sigma x(t)}{\varepsilon_0} \tag{1}$$

Where V_{oc}, σ, $x(t)$, and ε_0 are the Open-circuit voltage of MH-TENG, the charge density of the friction interfaces, the displacement distance of the FEP film, and the permittivity of vacuum. Hence, grinding the FEP friction surface with high mesh sandpaper is beneficial for MH-TENG to harvest sound energy. It is worth noting that sound-driven TENG is a contact-separation TENG and **Eq. 1** is based on a plate capacitor model. When it comes to sliding TENGs, it can be explained by a new model, which is edge approximation based equivalent capacitance (Li et al., 2019).

The working principle diagram of the TENG transducer is displayed in **Figure 1C**. The flexible FEP thin-film is forced to vibrate driven by the enhanced sound pressure. The contact-separation behavior between aluminum film and FEP film produces alternating currents. Firstly, as FEP film contacts with aluminum, the inner surfaces of FEP film and aluminum film produce an equal amount of opposite static charges. Specifically, the FEP friction surface is negatively charged and the aluminum surface is positively charged (**Figure 1Ci**). With the change of film tension and acoustic pressure, FEP film tends to leave the aluminum film, and the interface separation of positive and negative charges leads to the induced potential difference of the two electrodes. This difference can push the free electrons of the carbon electrode to flow to the aluminum electrode. In this process, the potentials tend to balance and positive charges are generated on the carbon electrode. (**Figure 1Cii**). The charge flow process continues to the maximum friction interface separation distance (**Figure 1Ciii**). When the direction of sound pressure changes, FEP film is pushed to aluminum film. The potential difference of the two electrodes gradually decreases, so unbound electric charges are transferred from the aluminum film to the carbon electrode (**Figure 1Civ**). As the two friction interfaces contact again, the charges distribution at the friction interface returns to the initial state with the disappearance of the potential difference. The above is a complete power generation cycle. **Figure 1D** shows the simulation results of potential changes during the contact-separation of FEP film and aluminum film by COMSOL software, which is consistent with the working principle of **Figure1C**. Obviously, MH-TENG produces AC output.

Acoustic Characteristics of Resonators

Helmholtz resonator is a typical acoustic resonator, which is used to eliminate noise in the industry (Zhang et al., 2015; Cai et al., 2017). However, when it comes to acoustic energy harvesting, the Helmholtz resonator shows excellent sound pressure amplification performance. An inflexible cavity and an open neck tube constitute a typical Helmholtz resonator. In theory, for low-frequency acoustics, the Helmholtz resonator is similar to

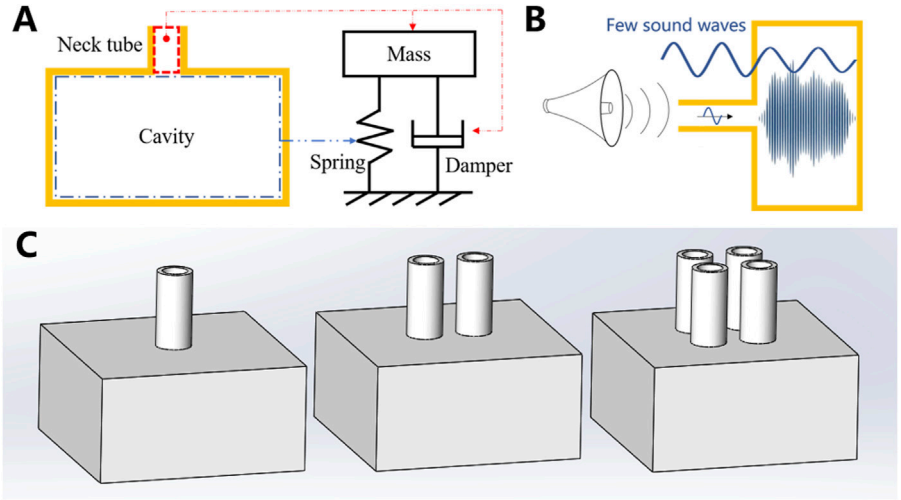

FIGURE 2 | (A) Mass spring damping system of the typical Helmholtz resonator **(B)** Propagation process of acoustic wave excitation through Helmholtz resonator **(C)** Structure diagrams of Helmholtz resonators with single tube, with dual tubes, and with four tubes.

a mass spring damping system (Pillai and Deenadayalan, 2014), as shown in **Figure 2A**. To be specific, the air within the tube is similar to a mass, the trapped air of the cavity becomes spring, and the heat loss and sound radiation caused by the air vibration of the tube come to be a damper. The characteristic frequency of this typical resonator is related to the cavity volume and neck tube parameters, and its equation is as follows:

$$f_{HR} = \frac{C}{2\pi}\sqrt{\frac{S}{VL_n}} \tag{2}$$

Where C is air sound velocity, S is the flow area of the neck tube, L_n is the equivalent length of the neck tube, and V is the volume of air inside the cavity. As displayed in **Figure 2B**, while sound waves are incident from the open end of the tube, the resonator can greatly increase the pressure of the sound waves and reach the highest sound pressure near the resonant frequency. It is worth noting that few low-frequency sound waves have powerful penetration, which has a definite impact on the sound pressure in the cavity, shown in subsequent experiments. Inspired by the broadband resonator structure used in the industrial noise elimination (Yu et al., 2008; Cai and Mak, 2018), an improved multi-tube parallel resonator is studied to maintain the sound pressure amplification effect in a wide frequency range. The acoustic characteristics of Helmholtz resonators with a single tube, with dual tubes, and with multi tubes are evaluated in this part. **Figure 2C** shows their structures.

To explore the acoustic characteristics of the improved multi-tube parallel Helmholtz resonators, a low-frequency speaker (woofer) is used to provide the sound power source. A digital function signal generator can accurately adjust the frequency of the sound wave and send out a sine wave. Besides, a power amplifier is used to control the intensity of the sound source. A sound level meter is installed at the opening of the tube to assess the incident sound waves, and another meter is installed on the side of the resonator cavity to monitor the amplified sound pressure level (SPL). **Figure 3** shows the responses of sound pressure levels (SPLs) inside of modified resonators to sound waves. This part studies the effect of different neck tube parameters, including length, diameter, number of neck tubes, and spacing of parallel neck tubes, on the acoustic performance of the improved resonator.

Figure 3A reveals the SPLs inside of Helmholtz resonators with different single tube lengths at the SPL of 94 dB. Not surprisingly, the SPL in a typical Helmholtz resonator is significantly amplified. With the increase of neck tube length, the sound pressure amplification effect of the resonator is slightly reduced, and the resonant frequency also decreases. The SPL of the resonator cavity with a 10 mm long neck tube is amplified by 18 dB, and that resonant frequency is 215 Hz. While the tube length extends to 30 mm, the resonant frequency decreases to 144 Hz, and that SPL is only amplified by 14 dB. As the incident sound waves rise to 100 dB, shown in **Figure 3B**, the sound pressure amplification of the resonator remains stable. To maintain the good low-frequency characteristics of the resonator, a 30 mm long neck tube is used in subsequent experiments. More notably, with the continuously increasing frequency of incident sound waves, the sound pressure magnifier function of the resonator disappears quickly and even plays a role in acoustic attenuation. As displayed in **Figure 3C,** the SPLs and resonant frequency of resonators have a positive correlation with the tube diameter, which is consistent with **Eq. 2**. **Figure 3D** shows the SPLs inside of dual-tube Helmholtz resonators with different neck tube spacings at 100 dB incident sound waves. In a range of approximately twice the resonant frequency, the dual-tube resonator has two distinct sound pressure level peaks, where the SPL can be amplified at both characteristic frequencies. The SPL of the first characteristic frequency is significantly greater than that of the second characteristic frequency. Results show that

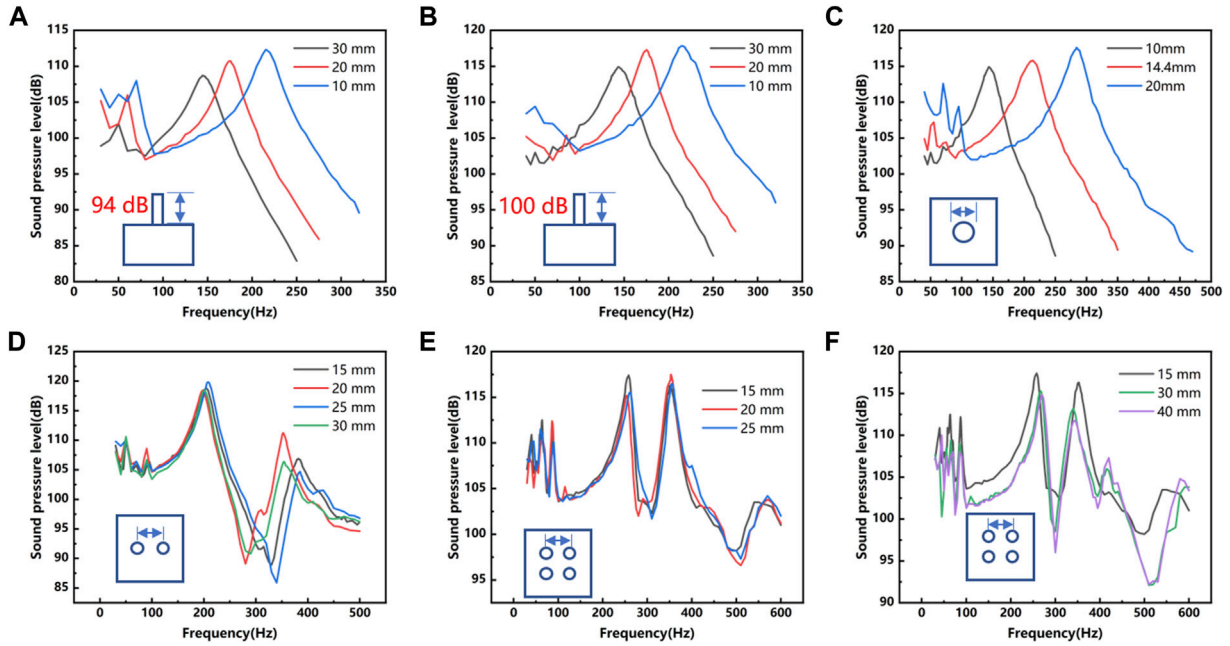

FIGURE 3 | Responses of sound pressure levels (SPLs) inside of modified resonators to sound waves **(A,B)** SPLs inside of the single tube Helmholtz resonators with different tube lengths under 94 and 100 dB incident sound waves, respectively **(C)** SPLs inside of the single tube Helmholtz resonators with different tube diameters under 100 dB incident sound waves **(D)** SPLs inside of dual-tube Helmholtz resonators with different tube spacings under 100 dB incident sound wave **(E,F)** SPLs inside of four-tube Helmholtz resonators with different tube spacings under 100 dB incident sound waves.

the neck tube spacing has a nonlinear effect on the characteristic frequency of the resonator, especially at the second characteristic frequency. When the spacing between two tubes is odd times of the tube radius, these resonators have the same resonant frequency, and the SPL of the resonator with a small spacing is slightly higher. The regular pattern of the resonator with tube spacing of even times radius is similar to the former, but the resonance frequency is lower.

Compared with a single tube Helmholtz resonator, the sound pressure amplification effect of a dual-tube Helmholtz resonator is significantly improved. As shown in **Figures 3B–D**, the SPL of a dual-tube resonator with a 25 mm tube spacing is amplified by 20 dB, while that of a single tube resonator is only amplified by 15 dB. In addition, the resonant frequency and bandwidth of the dual-tube resonator are larger than that of a single tube resonator. **Figures 3E,F** shows the SPLs inside of four-tube Helmholtz resonators with different neck tube spacings at 100 dB. In terms of the wide frequency range, the multi-tube Helmholtz resonator maintains a good sound pressure amplification effect. Within an acoustic frequency range of 480Hz, the SPL inside of a four-tube Helmholtz resonator is higher than 100dB. Interestingly, taking the amplified SPL of 6 dB as the standard, the bandwidth of a multi-tube resonator is about 2.2 times that of a single tube and 1.5 times that of dual tubes. The multi-tube resonator has two significant resonant frequencies. At these frequencies, two approximate high sound pressure levels are achieved. With a tube spacing of 15mm, the two maximum sound pressure levels of the multi-tube Helmholtz resonator are 116 and 117 dB, respectively. However, when the tube spacing is larger than 30 mm (3 times the tube diameter), the sound pressure amplification effect of the resonator decreases, and the resonant frequency changes. Therefore, a 20 mm tube spacing resonator was used in subsequent experiments to maintain a good sound pressure amplification effect and frequency bandwidth. Besides that, as shown in **Figures 3A–F**, some large sound pressure levels appear at sound wave frequencies below 100 Hz. These low-frequency sound waves have a strong penetration ability, illustrated in **Figure 2B**, which makes the sound waves enter the cavity through the front cover plate of the resonator and reflect in the cavity. In general, it is conducive to sound waves collection.

Performance of the Multi-Tube Parallel Helmholtz Resonator-Based Triboelectric Nanogenerator

The electricity generation performance of sound-driven MH-TENG is investigated in this part, as shown in **Figure 4**. The influencing factors include acoustic frequency and sound pressure. In addition, it also shows the dependence of MH-TENG power generation performance on the sound pressure amplification effect of the resonator. **Figure 4A** shows the schematic diagram of power generation experiments. The sinusoidal sound waves signal from the speaker (JBL) is provided by a digital signal generator (UTG-2062B) and magnified by a power amplifier (XY-200). The SPLs of the incident and amplified sound waves are measured by two GM1553 sound level meters. The electricity generation

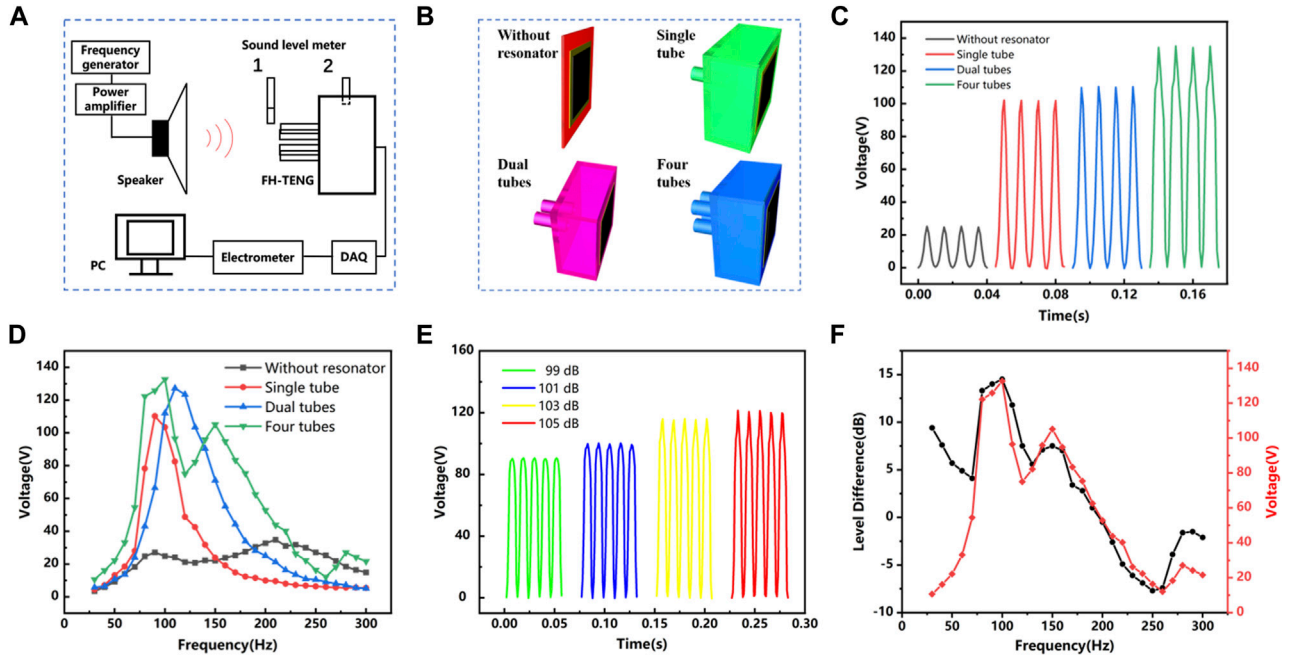

FIGURE 4 | Electricity generation performance experiments of sound-driven MH-TENG **(A)** Schematic diagram of power generation experiments **(B)** Schematic diagram of the TENGs without a resonator, with single-tube Helmholtz resonator, with dual-tube Helmholtz resonator, and with four-tube Helmholtz resonator. **(C)** V_{oc} of TENGs driven by the same incident sound waves **(D)** The peak V_{oc} of TENGs under a frequency range of 30–300 Hz **(E)** V_{oc} of the MH-TENG driven by the different incident sound waves pressures **(F)** Amplified sound pressure level difference and V_{oc} of the MH-TENG.

performances of MH-TENG, including open-circuit voltage (V_{oc}) signal, short-circuit current (I_{sc}) signal, and transferred charges (Q_{sc}) signal are gathered by an accurate electrometer (Keithley 6514).

Figure 4B displays the schematic diagram of the TENGs with single tube Helmholtz resonator, with dual-tube Helmholtz resonator, with four-tube Helmholtz resonator, and without a resonator. At a sound frequency of 100 Hz and a SPL of 106 dB, the open-circuit voltage (V_{oc}) of the above TENGs is shown in **Figure 4C**. As expected, the improved Helmholtz resonators effectively enhance the electricity generation performance of the sound-driven TENGs. The maximum V_{oc} of TENG without a resonator is only 22 V, and the voltage of single-tube resonator TENG is 100 V. Moreover, the maximum V_{oc} of the TENG with a dual-tube resonator increases to 110 V, and this value of MH-TENG ascends to 130 V. **Figure 4D** shows the peak V_{oc} of sound-driven TENGs under a frequency range of 30–300 Hz. With a typical Helmholtz resonator, the V_{oc} of TENG is heightened in a narrow frequency range. The maximum V_{oc} and the optimum frequency of this sound-driven TENG are 110 V and 90 Hz, respectively. As the acoustic frequency exceeds 90 Hz, the performance of TENG decreases rapidly. With a dual-tube resonator, the sound-driven TENG achieves the maximum voltage of 120 V under the incident sound waves of 110 Hz. Compared with a single-tube generation device, the dual-tube Helmholtz resonator TENG has a larger electrical output and a wider frequency range. Surprisingly, the peak of the second characteristic frequency of the dual-tube resonator disappears. This represents the influence of a flexible thin-film TENG transducer on the sound energy collection device. In addition, MH-TENG presents a unique electrical output characteristic, which is similar to the acoustic characteristics of a four-tube Helmholtz resonator. The open-circuit voltage of MH-TENG reaches two peaks at the acoustic frequency of 100 and 150 Hz, which are 130 and 105 V, respectively. Although the peak of the second characteristic frequency is also reduced, this characteristic significantly widens the frequency band of MH-TENG. The experimental results show that MH-TENG can effectively increase the generation performance of TENG within the bandwidth of about 230 Hz. This frequency bandwidth represents the bandwidth in which the power generation performance of MH-TENG is superior to that of the TENG transducer, shown in **Supplementary Figure S1**. Compared with single-tube and dual-tube resonator TENGs, the working bandwidth of MH-TENG is expanded by 130 and 77% respectively. Referring to relevant literatures, MH-TENG has the widest working frequency bandwidth (**Supplementary Table S1**). More significantly, the application of thin-film TENG has vastly changed the acoustic characteristics of the resonator, and the optimal working frequency of TENGs based on the resonator is reduced to about 100 Hz. The rigid structure of the resonator is changed by the flexible thin-film TENG.

Figure 4E shows the MH-TENG voltage output driven by different sound pressures. With the increase of sound pressure, the electrical output of MH-TENG increases. This is because the increase of sound pressure strengthens the contact stress and area of the FEP film, which produces more charges. **Figure 4F** shows the amplified sound pressure level difference and voltage output

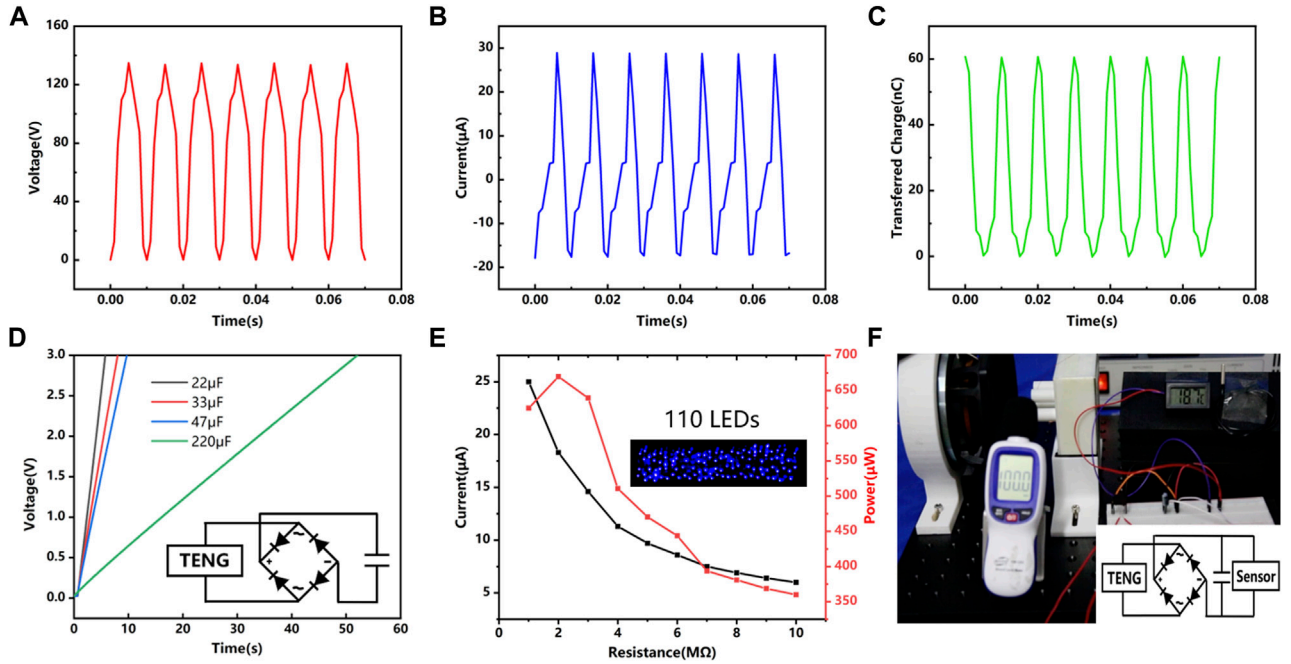

FIGURE 5 | (A) The V_{oc} **(B)** I_{sc}, and **(C)** Q_{sc} of MH-TENG driven by sound waves of 100 Hz and 106 dB **(D)** Charging performance of different capacitors powered by MH-TENG **(E)** Resistance matching test experiment of MH-TENG **(F)** Demonstration of MH-TENG supplying power to an electronic thermometer.

of the MH-TENG, which maintain a similar trend. The sound pressure level difference refers to the difference between the amplified SPL in the cavity and the SPL of incident sound waves. This trend clarifies that the performance of MH-TENG obviously depends on the sound pressure amplification effect of the resonator. However, at some frequencies, the output of MH-TENG is greatly affected by the TENG transducer. As the acoustic frequency is lower than 70 Hz, the penetration ability is puissant, and more sound energy passes through the FEP film. In addition, the low frequency (<50 Hz) is far from the optimal vibration frequency of the FEP film. As a result, it is hard for the thin film of the TENG transducer to vibrate well. Therefore, the design of a sound energy harvesting device needs to consider the frequency characteristics of the resonator and transducer at the same time.

The MH-TENG can be used as a low-frequency and broadband sound energy harvesting device to provide energy for small electronics. As shown in **Figures 5A–C**, under the incident sound waves of 106 dB and 100 Hz, the V_{oc}, I_{sc}, and Q_{sc} of MH-TENG can reach 135 V, 29 μA, 61 nC, respectively. **Figure 5D** shows the charging performance of the MH-TENG for different capacities. The alternating current produced by MH-TENG is stored in capacitors via the elementary rectifier bridge circuit. The results indicate that a 22 μF capacitor powered by the MH-TENG can be charged to 3 V within 5 s. And the 220 uF capacitor takes only 52 s to be charged from 0 to 3 V. **Figure 5E** shows the MH-TENG load resistance matching experiment. The MH-TENG achieves a maximum power of about 670 μW at 2 MΩ. In addition, **Figure 5E** and **Supplementary Video S1** show that MH-TENG can directly supply energy to 110 LEDs. What's more, benefitting from the good capacitor charging performance, the sound-driven MH-TENG can supply power to low-power sensors. As illustrated in **Figure 5F** and **Supplementary Video S2**, an electronic thermometer is activated, when the MH-TENG charges a 220 μF capacitor to about 1.6 V within 13 s.

CONCLUSION

In summary, the study has proposed a broadband sound-driven TENG based on a multi-tube Helmholtz resonator to harvest low-frequency sound energy. Before that, we clarified the effect of neck tube parameters on the acoustic characteristics of Helmholtz resonators. When the resonator cavity is fixed, the resonant frequency and pressure amplification effect of the resonator increase with the decrease of the tube length. In addition, tube spacing also affects the resonator. For the dual-tube Helmholtz resonator, when the tube spacing is odd times of the neck tube radius, the resonator's resonant frequency is slightly less than that of even times, which is obvious at the second resonant frequency. Besides, the SPL of the first resonant frequency is significantly greater than that of the second resonant frequency. As for a four-tube Helmholtz resonator, the relationship between frequency and sound pressure level presents two modes with approach peak values, which significantly widens the working frequency band of the resonator. However, this advantage disappears when the tube spacing is too large (greater than 3 times tube diameters). The application of a multi-tube Helmholtz resonator makes the MH-TENG obtain a better output

performance, which has a wide working frequency band. In general, the MH-TENG can significantly improve the output performance over the 230 Hz frequency bandwidth range. Compared with the single tube resonator TENG and the dual-tube resonator TENG, the power generation performance of MH-TENG is significantly increased, and the working frequency bandwidth is expanded by 130 and 77%, respectively. Besides, the MH-TENG has a good capacitor charging performance. It only takes 52 s for a 220 μF capacitor to be charged from 0 to 3 V. The MH-TENG has also demonstrated its capability of powering 110 LEDs and an electronic thermometer. Therefore, the MH-TENG could be a great addition to low power appliances in machinery factories, railways, engine rooms, and other high noise environments.

DATA AVAILABILITY STATEMENT

The data presented in this study are available on request from the corresponding author.

AUTHOR CONTRIBUTIONS

QZ: Conceptualization, validation, writing original draft preparation, writing-review and editing. ZX: Conceptualization, validation. YW: Software, visualization. LL: Validation, investigation. HY: Investigation. HW: Writing original draft preparation. MX: Conceptualization, supervision.

FUNDING

The work was supported by Project of Dalian Outstanding Young Scientific and Technological Personnel (2021RJ11).

SUPPLEMENTARY MATERIAL

The Supplementary Material for this article can be found online at: https://www.frontiersin.org/articles/10.3389/fmats.2022.896953/full#supplementary-material

REFERENCES

Ali, S. A. (2011). Industrial Noise Levels and Annoyance in Egypt. *Appl. Acoust.* 72, 221–225. doi:10.1016/j.apacoust.2010.11.001

Cai, C., and Mak, C. M. (2018). Acoustic Performance of Different Helmholtz Resonator Array Configurations. *Appl. Acoust.* 130, 204–209. doi:10.1016/j.apacoust.2017.09.026

Cai, C., Mak, C. M., and Wang, X. (2017). Noise Attenuation Performance Improvement by Adding Helmholtz Resonators on the Periodic Ducted Helmholtz Resonator System. *Appl. Acoust.* 122, 8–15. doi:10.1016/j.apacoust.2017.02.006

Cui, N., Gu, L., Liu, J., Bai, S., Qiu, J., Fu, J., et al. (2015). High Performance Sound Driven Triboelectric Nanogenerator for Harvesting Noise Energy. *Nano Energy* 15, 321–328. doi:10.1016/j.nanoen.2015.04.008

Dukhin, A. S., and Goetz, P. J. (2009). Bulk Viscosity and Compressibility Measurement Using Acoustic Spectroscopy. *J. Chem. Phys.* 130, 124519. doi:10.1063/1.3095471

Huabing, W., Xiaojia, W., Junjie, W., Chengwei, C., and Zhiyuan, L. (2018). Noise Prediction and Control in a Cruise Ship. *IOP Conf. Ser. Mater. Sci. Eng.* 439, 032072. doi:10.1088/1757-899x/439/3/032072

Iftikhar Ahmad, A., Hassan, A., Anjum, M. U., Malik, S., and Ali, T. (2019). Ambient Acoustic Energy Harvesting Using Two Connected Resonators with Piezoelement for Wireless Distributed Sensor Network. *Acoust. Phys.* 65, 471–477. doi:10.1134/s1063771019050014

Izhar, and Khan, F. U. (2018). Electromagnetic Based Acoustic Energy Harvester for Low Power Wireless Autonomous Sensor Applications. *Sr* 38, 298–310. doi:10.1108/sr-04-2017-0062

Ji, X., Yang, L., Xue, Z., Deng, L., and Wang, D. (2020). Enhanced Quarter Spherical Acoustic Energy Harvester Based on Dual Helmholtz Resonators. *Sensors* 20, 7275. doi:10.3390/s20247275

Jun Hong, Z., and Bing, H. (2005). Analysis of Engine Front Noise Using Sound Intensity Techniques. *Mech. Syst. Signal Process.* 19, 213–221. doi:10.1016/j.ymssp.2004.03.007

Khan, F. U., and Izhar (2016). Electromagnetic Energy Harvester for Harvesting Acoustic Energy. *Sādhanā* 41, 397–405. doi:10.1007/s12046-016-0476-9

Kim, Y., Na, J., Park, C., Shin, H., and Kim, E. (2015). PEDOT as a Flexible Organic Electrode for a Thin Film Acoustic Energy Harvester. *ACS Appl. Mater. Inter.* 7, 16279–16286. doi:10.1021/acsami.5b02762

Li, X., Lau, T. H., Guan, D., and Zi, Y. (2019). A Universal Method for Quantitative Analysis of Triboelectric Nanogenerators. *J. Mater. Chem. A.* 7, 19485–19494. doi:10.1039/c9ta06525c

Li, X., Xu, G., Xin, X., Fu, J., and Zi, Y. (2018). Standardization of Triboelectric Nanogenerators: Progress and Perspectives. *Nano Energy* 56, 40–55. doi:10.1016/j.nanoen.2018.11.029

Liu, J., Cui, N., Gu, L., Chen, X., Bai, S., Zheng, Y., et al. (2016). A Three-Dimensional Integrated Nanogenerator for Effectively Harvesting Sound Energy from the Environment. *Nanoscale* 8, 4938–4944. doi:10.1039/c5nr09087c

Luo, J. J., and Wang, Z. L. (2020). Recent Progress of Triboelectric Nanogenerators: From Fundamental Theory to Practical Applications. *Ecomat* 2, e12059. doi:10.1002/eom2.12059

Noh, H.-M. (2018). Acoustic Energy Harvesting Using Piezoelectric Generator for Railway Environmental Noise. *Adv. Mech. Eng.* 10, 168781401878505. doi:10.1177/1687814018785058

Pillai, M. A., and Deenadayalan, E. (2014). A Review of Acoustic Energy Harvesting. *Int. J. Precis. Eng. Manuf.* 15, 949–965. doi:10.1007/s12541-014-0422-x

Qiu, W., Feng, Y., Luo, N., Chen, S., and Wang, D. (2020). Sandwich-like Sound-Driven Triboelectric Nanogenerator for Energy Harvesting and Electrochromic Based on Cu Foam. *Nano Energy* 70, 104543. doi:10.1016/j.nanoen.2020.104543

Song, W. Z., Qiu, H. J., Zhang, J., Yu, M., Ramakrishna, S., Wang, Z. L., et al. (2021). Sliding Mode Direct Current Triboelectric Nanogenerators. *Nano Energy* 90, 106531. doi:10.1016/j.nanoen.2021.106531

Wang, Z. L., Chen, J., and Lin, L. (2015). Progress in Triboelectric Nanogenerators as a New Energy Technology and Self-Powered Sensors. *Energy Environ. Sci.* 8, 2250–2282. doi:10.1039/c5ee01532d

Wang, Z., Wu, Y., Jiang, W., Liu, Q., Wang, X., Zhang, J., et al. (2021). A Universal Power Management Strategy Based on Novel Sound-Driven Triboelectric Nanogenerator and its Fully Self-Powered Wireless System Applications. *Adv. Funct. Mater.* 31, 2103081. doi:10.1002/adfm.202103081

Yang, J., Chen, J., Liu, Y., Yang, W., Su, Y., and Wang, Z. L. (2014). Triboelectrification-based Organic Film Nanogenerator for Acoustic Energy Harvesting and Self-Powered Active Acoustic Sensing. *ACS Nano* 8, 2649–2657. doi:10.1021/nn4063616

Yu, G., Li, D., and Cheng, L. (2008). Effect of Internal Resistance of a Helmholtz Resonator on Acoustic Energy Reduction in Enclosures. *The J. Acoust. Soc. America* 124, 3534–3543. doi:10.1121/1.2996328

Yuan, H., Yu, H., Liu, X., Zhao, H., Zhang, Y., Xi, Z., et al. (2021). A High-Performance Coniform Helmholtz Resonator-Based Triboelectric Nanogenerator for Acoustic Energy Harvesting. *Nanomaterials* 11, 3431. doi:10.3390/nano11123431

Yuan, M., Cao, Z., Luo, J., and Pang, Z. (2018). Low Frequency Acoustic Energy Harvester Based on a Planar Helmholtz Resonator. *AIP Adv.* 8, 085012. doi:10.1063/1.5042683

Yuan, M., Li, C., Liu, H., Xu, Q., and Xie, Y. (2021). A 3D-Printed Acoustic Triboelectric Nanogenerator for Quarter-Wavelength Acoustic Energy Harvesting and Self-Powered Edge Sensing. *Nano Energy* 85, 105962. doi:10.1016/j.nanoen.2021.105962

Yuan, M., Sheng, X., Cao, Z., Pang, Z., and Huang, G. (2020). Joint Acoustic Energy Harvesting and Noise Suppression Using Deep-Subwavelength Acoustic Device. *Smart Mater. Struct.* 29, 035012. doi:10.1088/1361-665x/ab6697

Zhang, Z., Zhao, D., Han, N., Wang, S., and Li, J. (2015). Control of Combustion Instability with a Tunable Helmholtz Resonator. *Aerospace Sci. Techn.* 41, 55–62. doi:10.1016/j.ast.2014.12.011

Zhao, H., Xiao, X., Xu, P., Zhao, T., Song, L., Pan, X., et al. (2019). Dual-Tube Helmholtz Resonator-Based Triboelectric Nanogenerator for Highly Efficient Harvesting of Acoustic Energy. *Adv. Energ. Mater.* 9, 1902824. doi:10.1002/aenm.201902824

Zhu, J., Liu, X., Shi, Q., He, T., Sun, Z., Guo, X., et al. (2019). Development Trends and Perspectives of Future Sensors and MEMS/NEMS. *Micromachines* 11, 7. doi:10.3390/mi11010007

Zou, H., Zhang, Y., Guo, L., Wang, P., He, X., Dai, G., et al. (2019). Quantifying the Triboelectric Series. *Nat. Commun.* 10, 1427. doi:10.1038/s41467-019-09461-x

Zou, Y., Raveendran, V., and Chen, J. (2020). Wearable Triboelectric Nanogenerators for Biomechanical Energy Harvesting. *Nano Energy* 77, 105303. doi:10.1016/j.nanoen.2020.105303

Zou, Y., Xu, J., Chen, K., and Chen, J. (2021). Advances in Nanostructures for High-Performance Triboelectric Nanogenerators. *Adv. Mater. Technol.* 6, 2000916. doi:10.1002/admt.202000916

Conflict of Interest: The authors declare that the research was conducted in the absence of any commercial or financial relationships that could be construed as a potential conflict of interest.

Publisher's Note: All claims expressed in this article are solely those of the authors and do not necessarily represent those of their affiliated organizations, or those of the publisher, the editors and the reviewers. Any product that may be evaluated in this article, or claim that may be made by its manufacturer, is not guaranteed or endorsed by the publisher.